Compact 480-GHz Radiometer Calibration Unit With Specular Reflection Absorber for Atmospheric Remote Sensor On-Board Microsatellite

Maho Nakagawa, Yuki Uchiyama, Takayoshi Yamada, Toshiyuki Nishibori, Satoshi Ochiai, Maya Mizuno, Akihisa Uematsu, Shigeru Sato, Yukio Nakano, and Yasuko Kasai

***Abstract*—In this study, an on-board calibration hot load (CHL) unit was developed for a terahertz sensing system (THzSens) receiver at 480 GHz to observe the emission lines of water and oxygen in the atmosphere. The compact CHL unit can be mounted on a microsatellite. We propose an accurate calibration method and a unit compact in design. We conducted experiments in order to obtain the best possible return loss value below the required −60 dB for calibration. The CHL unit uses two specular reflection absorber (SRA) plates and a radar absorbing material (RAM) as the absorber termination. The absorbers are assembled in a lightweight case made of carbon-fiber-reinforced plastics. The SRAs are placed at the Brewster angle with respect to the incident radiation to minimize reflection, which was found experimentally at 480 GHz. The CHL design is expected to have less than −78 dB reflection loss including SRA back scattering at 480 GHz. The return loss as a function of frequency for this design is below −60 dB, meeting the design requirements. Further, a compact prototype CHL was manufactured based on the proposed quasi-optical design. The new CHL for 480 GHz is 1/10 in the volume of the previous SMILES CHL for 650 GHz. The manufactured CHL prototype will be evaluated as a calibrator using the transmitter/receiver setup used in this study.**

***Index Terms*—Absorbing media, calibration, satellites, terahertz radiation.**

Manuscript received August 21, 2020; revised December 18, 2020 and January 28, 2021; accepted March 5, 2021. Date of publication July 7, 2021; date of current version September 2, 2021. This work was supported in part by the "Research and Development program on key technology in terahertz frequency bands" of the Ministry of Internal Affairs and Communications under Grant JPJ000254. *(Corresponding author: Maho Nakagawa.)*

Maho Nakagawa, Yuki Uchiyama, Takayoshi Yamada, and Shigeru Sato are with the Terahertz Technology Research Center, National Institute of Communication and Technology, Tokyo 184-8795, Japan (e-mail: nakagawa66@nict.go.jp; b142309y@st.u-gakugei.ac.jp; yamada-takayoshi@nict.go.jp; sato-shigeru@nict.go.jp).

Toshiyuki Nishibori and Akihisa Uematsu are with the Japan Aerospace Exploration Agency, Tsukuba 305-8505, Japan (e-mail: nishibori.toshiyuki@jaxa.jp; uematsu.akihisa@jaxa.jp).

Satoshi Ochiai and Maya Mizuno are with the Applied Electromagnetic Research Institute, National Institute of Information and Communications Technology, Tokyo 184-8795, Japan (e-mail: ochiai@nict.go.jp; mmizuno@nict.go.jp).

Yukio Nakano is with the Department of Environmental Sciences, Tokyo Gakugei University, Tokyo 184-8501, Japan (e-mail: nakano@u-gakugei.ac.jp).

Yasuko Kasai is with the Terahertz Technology Research Center, National Institute of Communication and Technology, Tokyo 184-8795, Japan, and also with the Physics Program at the Graduate School of Pure and Applied Sciences, Tsukuba University, Tsukuba 305-8577, Japan (e-mail: ykasai@nict.go.jp).

Color versions of one or more figures in this article are available at https://doi.org/10.1109/TTHZ.2021.3095436.

Digital Object Identifier 10.1109/TTHZ.2021.3095436

I. Introduction

MICROWAVE satellites have served an important role in quantifying Earth's minor atmospheric components. Some examples of earth observing satellites are the Advanced Microwave Scanning Radiometer for the Earth Observing System (AMSR-E) [1], the Microwave Humidity Sounder (MHS) [2], the Earth Observing System Microwave Limb Sounder (EOS MLS) [3], and the Superconducting Submillimeter-Wave Limb-Emission Sounder (SMILES) [4]. The AMSR-E and MHS operate at low frequencies. The AMSR-E carries a microwave radiometer operating at 6.925, 10.65, 18.7, 23.8, 36.5, and 89 GHz with a calibration warm load, which enables the global observation of water phases, such as water vapor. The MHS has an across-track scanning microwave heterodyne radiometer operating five channels in the 89–190 GHz band, allowing the device to observe water vapor at increased heights in the troposphere. Complementary, MLS and SMILES operate at high frequencies. The EOS MLS has heterodyne radiometers to measure atmospheric chemical species such as OH, HO_2, H_2O, O_3, HCl, ClO, HOCl, BrO, HNO_3, N_2O, CO, HCN, CH_3CN, and volcanic SO_2 around 118, 190, 240, and 640 GHz, and 2.5 THz. On the other hand, SMILES operated at 625–650 GHz as a heterodyne radiometer, providing the vertical distribution profiles of species such as O_3, HCl, ClO, HOCl, HO_2, HNO_3, CH_3CN, and BrO from the stratosphere to the mesosphere. Several microwave class sensors have a mass in the 500 kg class, size in the 1–3 m class, and require a large satellite-bus or the international space station (ISS).

For instruments in the terahertz (THz) frequency range, it is feasible to construct a sensor of compact size, light weight, and with high frequency resolution. Passive observation, being less demanding in power consumption than active observation, can successfully accommodate such a compact sensor. It is possible to mount THz sensing system (THzSens) weighing only a few kg on 50 kg class microsatellites, reducing the launch cost dramatically from a few hundred million Euro to a few million Euro and thereby making space more accessible, both within Earth's orbit and in planetary exploration. It is interesting to note that the THz regime is the only frequency region to realize the observation of oxygen (O_2) and water (H_2O) simultaneously at 480 GHz in a range of few GHz. This capability is for example crucial to understand the daytime and nighttime

climate of the atmosphere of Mars [5]–[11] (using simulation results of the general circulation model of Mars from the Mars Climate Database [12]–[14]). Our purpose is to make a common standard THzSens receiver including a calibration subsystem for observation geometry of both up-looking and limb sounding.

The THz frequency range is typically defined as the submillimeter range from 300 to 3000 GHz [15]. We focus on the 0.48 THz (480 GHz) region to observe the height distribution of H_2O and O_2 abundance simultaneously in the Earth and planetary atmosphere in a range of 1 GHz via passive heterodyne detection by means of previous work [16], [17].

The THzSens components should be compact to enable installation on a microsatellite. In this study, the size of the microsatellite unit envelope is required to be less than one cubic meter. The maximum allowable mass is less than 100 kg, and the total mass of the components of the payload bus assumes approximately 70 kg [18]. The THzSens receiver needs to be calibrated regularly to determine the emission spectrum of the molecules accurately. The calibration requires two reference points in the output power of the receiver (intensity) and brightness-temperature domains. A calibration hot load (CHL) unit is used as the hot reference. In the case of SMILES [4], [19], the blackbody calibration system consists of three specular reflection absorbers (SRAs) and a radar absorbing material (RAM) as an absorber termination. Our CHL unit is using a similar design, but with only two SRA plates. This CHL type has a lot of advantages because of the simplicity of surface fabrication related to the reflection loss and the simplicity of the thermal design [20]. The calibrator of SMILES has low reflectivity, and the sensor can precisely measure the levels of several stratospheric trace gases. In this study, the SMILES calibration system was too large (the payload size being $80 \times 100 \times 180$ cm^3) to be modified directly for use on a microsatellite. The entire receiver, including components of the CHL unit, must have a size less than $50 \times 50 \times 50$ cm^3 and mass less than 30 kg. The receiver payload is composed of a submillimeter antenna, a submillimeter mixing unit, an intermediate-frequency (IF) subsystem section, spectrometer, a central processing unit (data handling and power supply unit), and a CHL unit. The required volume and weight of the CHL unit were approximately 512 cm^3 and 0.4 kg, respectively. In this way, the volume is approximately 1/10 that of SMILES (4.816×10^3 cm^3) [4].

Our proposed CHL design with only two SRA plates leads to a more compact design. In previous work [4], the return loss of the SMILES CHL module was much less than -60 dB ($f = 640$ GHz). In addition, a conical target module coated with a 3.0-mm-thick layer of Eccosorb CR110 (manufactured by Emerson and Cuming, Inc., Canton, MA) was designed for the European Space Agency mission achieved a return loss of approximately -70 dB between 200 and 700 GHz [21].

The radiometer minimum detectable temperature can be evaluated for double side band (DSB) by the following equation [4]:

$$T_{rms} = \frac{2T_{sys}}{\sqrt{B \cdot \tau}} \tag{1}$$

where $2T_{sys}$ (= 3000 K) is the system noise temperature for DSB, B (= 100 kHz) is the detection noise bandwidth and τ (= 0.5 s) is the integration time. We considered a method based on the r_{cal} term in [4] of only the calibrator indices for decreasing the return loss (*RL*) of the standing wave amplitude from the calibration source. The thermal emissions of the CHL requires a return loss less than –48 dB, for cases in which the thermal variation contribution of the receiver components after the horn can be neglected. For the actual observation, the noise temperature of the object should be considered. The lower limit of insertion loss was set conservatively in order to eliminate these hidden error factors. For example, if this device was used to explore a planet such as Mars, the temperature of the water vapor line at 474.7 GHz is approximately 100 K in the Mars atmosphere, our requirement was set as less than –60 dB. The focus of this study was on the development of a compact calibration system for the THzSens receiver using only two SRA plates and a RAM termination. Multiple reflections of THz radiation result in standing waves between the horn antenna and blackbody absorber [20], [22], [23]. These standing waves from multiple reflections cause errors in the two reference points determined by the calibration. Complete absorption of the incident thermal radiation is required for a high CHL performance. Therefore, the CHL unit should have optimized angles settings that minimize the surface reflectivity of the SRA as controlled by a two-phase stepper motor.

The aim of this study was to obtain the Brewster angle of the SRA. Due to the constraints of the stepping motor, the angle of the CHL was discretely set with a resolution of 1.8°. The Brewster angle was measured from a feasible CHL resolution using the stepper motor method. In addition, the CHL reflectivity at approximately 480 GHz, and the optimized Brewster angle, was evaluated using a quasi-optical reflectometer setup. We have conducted experiments to obtain the "best possible" return loss value for the CHL within the size and mass constraints of the mission. The remainder of this article is organized as follows.

Section II introduces the fundamental functions of the CHL unit. Section III briefly describes the CHL unit design for the THzSens. Section IV discusses the experiments performed to determine the Brewster angle for the SRA at 480 GHz. Section V presents the reflection loss at the Brewster angle for the THzSens receiver in the THz region. Finally, Section VI summarizes the conclusions and scope of future work.

II. Fundamental Theory

This section introduces the proposed method based on the Rayleigh–Jeans approximation. In this study, the CHL is composed of two SRA plates and a RAM as an absorber termination. The CHL unit needs to be designed to attain a low-reflectivity. A brief description of the numerical verification method for the design is therefore presented.

A. Calibration Method

An accurate calibration process is required for the observation of the atmospheric spectrum at an arbitrary frequency. In this study, the arbitrary frequency is set to 480 GHz. The receiver constantly alternates between the atmosphere, CHL, and cold sky. The CHL unit serves an important function in the receiver.

The brightness temperature in the Rayleigh–Jeans approximation (Rayleigh–Jeans brightness temperature) is given by

$$T_B\ (\nu, T)\ =\ \frac{c^2}{2k\nu^2} I \tag{2}$$

where I is the radiation intensity from the receiver (observed spectral intensity), ν is the frequency, c is the speed of light, k is Boltzmann constant, and T_B is the brightness temperature [24]. If the THzSens is mounted on an orbiting satellite, the hot load and cold view are used as reference points. The known brightness temperatures from these loads are used to compute the observed spectral intensity under the assumption that each brightness temperature and the thermal emission intensity have a linear relationship [25]. The thermal emissions of the hot and cold loads are from the blackbody and cold-sky view ($T_{B\_cold} = 4\ \mathrm{mK}$), respectively. From the equilibrium of radiant energy, the calibration source absorbs and emits radiation simultaneously. The error in the physical temperature has an influence on the error in the brightness temperature. The thermometers were embedded inside all absorbers and display the physical temperature at the first SRA, thus allowing for the radiant intensity to be obtained from the blackbody loads in the CHL calibrator.

B. Brewster Angle and Planewave Reflection at the Dielectric Surface

In the case wherein the blackbody is a perfect absorber in theory, a fraction of the thermal emission is reflected in reality. This reflection produces an error in the measured reference points caused by standing waves, which are present between the calibration system and horn antenna. Therefore, blackbody targets for calibration systems need to minimize reflections in the operating frequency range in the direction of the horn antenna.

A relationship was identified between the power reflection coefficient at the angle of incidence and the dielectric constant using the following Fresnel equations:

$$R\mathrm{s}\,(\nu,\ \theta)\ =\ \left|\frac{\cos\theta\ -\ \sqrt{\varepsilon\ -\sin^2\theta}}{\cos\theta\ +\ \sqrt{\varepsilon\ -\sin^2\theta}}\right|^2 \tag{3}$$

$$R\mathrm{p}\,(\nu,\ \theta)\ =\ \left|\frac{\varepsilon\cos\theta\ -\ \sqrt{\varepsilon\ -\sin^2\theta}}{\varepsilon\cos\theta\ +\ \sqrt{\varepsilon\ -\sin^2\theta}}\right|^2 \tag{4}$$

where R_s and R_p represent the reflection in the plane of incidence for which the polarization is perpendicular and parallel, respectively, θ is the incident angle with respect to the surface, and ε is the dielectric constant of an absorbing material [26]. It is assumed that the Fresnel Equations describe the reflection at an interface of a dielectric layer with infinite thickness. In the CHL, the thermal emission was reduced due to the minimum reflection angle input with the vertical polarization, called the Brewster angle. In particular, the two SRA plates in the CHL unit should be oriented at the approximate Brewster angle to reduce reflection. Further information on the CHL design is described in the following section. The real parts of ε and refractive index n are related by $n = \sqrt{\varepsilon}$, and from (4), the reflection coefficient with vertical polarization can be expressed as follows:

$$R_p\ =\ \left(\frac{n\cos\theta\ -\ \sin\theta}{n\cos\theta\ +\ \sin\theta}\right)^2. \tag{5}$$

Furthermore, the Brewster angle can be obtained indirectly by finding the minimum R_p in (5). The local minimum is, by definition, the point at which the derivative is zero. The low reflection angle of the horizontal (p)-polarized light (with vertical polarization with respect to the plane of incidence) was obtained by taking the derivative with respect to θ. It can be shown that the Brewster angle can be expressed as $\tan\theta = n$.

The Brewster angle can also be obtained by measuring the reflection coefficient directly at different angles of incidence. The *RL* is the magnitude of the power reflection coefficient from (3) and (4) in decibels and can be expressed as follows:

$$RL_{\mathrm{s}} = 10\log_{10}\left(R_{\mathrm{s}}\left(\nu,\theta\right)\right) \tag{6}$$

$$RL_{\mathrm{p}} = 10\log_{10}\left(R_{\mathrm{p}}\left(\nu,\theta\right)\right). \tag{7}$$

As mentioned in the preceding section, the CHL unit for the THzSens is required to have an RL_{p} of less than -60 dB.

III. Design of Calibration Target

This section summarizes the CHL design concept and provides a brief overview of the receiver for the THzSens. The design focus was the installation of a compact receiver on the microsatellite. This CHL unit is developed with a focus on the minimizing size and weight.

Fig. 1(a) shows a schematic overview of the proposed CHL unit and the THzSens receiver sensor for the microsatellite. The receiver has dimensions of $50 \times 50 \times 50$ cm^3, a maximum mass of 30 kg, and a total power consumption of less than 30 W. The CHL unit has the following design parameters: 1) a reduced number of absorbers to minimize space and 2) lightweight housing. The CHL unit provides two SRAs with 3.0-mm-thick plates and a RAM as an absorber termination. The first SRA has a back-to-back configuration, where different surface materials can easily be employed as reflectors/absorbers of incident radiation by a two-phase stepper motor (Tamagawa Seiki Co., Ltd, TS3692N1). During observation, the reflector mirror is set at an angle of 45.0°, the receiver can detect incident thermal radiation from the atmosphere. During calibration, the SRA is set at a suitable angle to minimize the reflection of radiation coming from outside using a two-phase stepper motor.

The parameter θ represents the incident angle of the radiation with respect to the SRA surface. The SRA uses the commercial MF110 plate manufactured by E&C Engineering, whereas the RAM is a pyramidal surface type absorbing material from the commercial TK-RAM by *Thomas Keating Ltd*. The reflector mirror at the back of the first SRA is made of a highly reflective aluminum plate. As shown Fig. 1(b), the incidental surfaces of the first and second SRAs of the CHL design are orthogonal to each other at an optimized angle. The vertical (s)-polarized beam of incident thermal radiation relative to the first SRA becomes a p-polarized beam relative to the second.

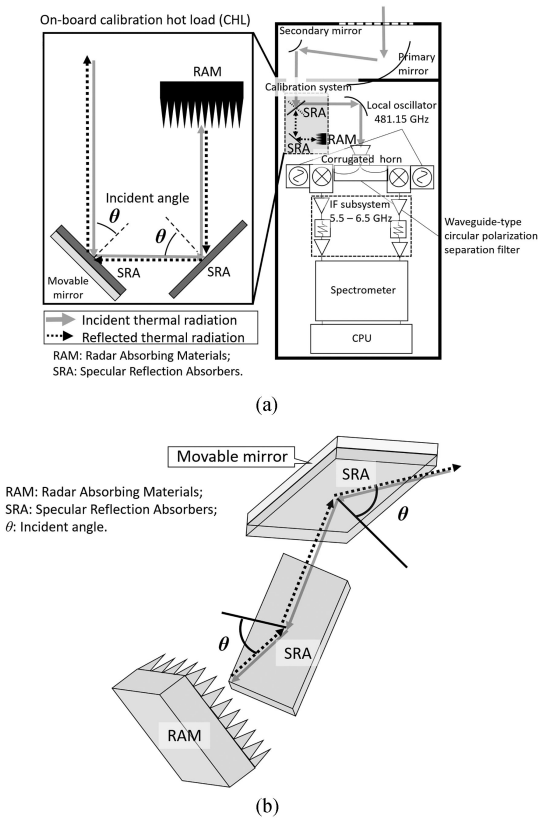

Fig. 1. (a) Schematic view of the CHL unit and entire receiver sensor of the microsatellite for the THzSens receiver system. (b) Three-dimensional model of the unit.

The mass of the fixed materials for the absorber in the calibration system was reduced by using carbon-fiber-reinforced plastics (CFRPs) instead of aluminum alloy. The CHL housing is also composed of CFRP materials to decrease the total mass. After implementing these weight-reducing design parameters, the volume and mass of the CHL unit were less than 512 cm^3 and 0.4 kg, respectively.

This receiver allows the measurement of water and oxygen emission lines using heterodyne techniques across two frequency bands: 486.64–487.64 GHz (upper sideband: USB) and 475.64–474.64 GHz (lower sideband: LSB). The THz radiation from outside the atmosphere reaches the spectrometer unit with or without passing through the CHL unit. For calibration, the radiation from deep space was used as the cold load and the CHL unit as the hot load. During the observation, the radiation pass into the corrugated horn without passing through the CHL unit. In our receiver configuration, an oven-controlled 100 MHz crystal oscillator and phase-locked dielectric 13.365 GHz resonator oscillator are used to generate the local oscillator (LO) source. The LO signal is multiplied to 240 GHz by an integrated amplifier multiplier chain (IAMC). The 480 GHz DSB subharmonic mixer, which is provided with sufficient pump power by the IAMC, is used to downconvert the radio frequency input signal to the IF. The input signal is mixed down to an IF of 6 GHz [17], and it is amplified and digitized by a compact spectrometer.

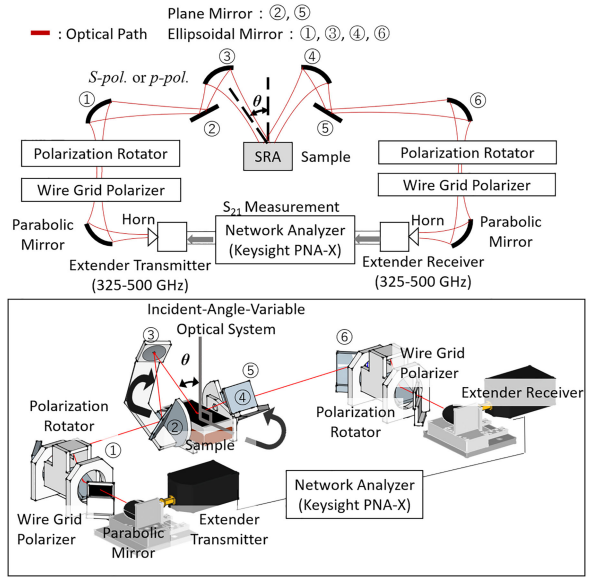

Fig. 2. Setup used to measure the setting angle of the SRA plate. The setup is based on the quasi-optical bench to allow measurement of the Brewster angle.

IV. Reflectivity of the SRA at Brewster Angle

This section shows the reflectivity measurements for the specular reflectivity absorber plates at the optimized angles introduced in the previous section. The reflected signal is excessively close to the noise floor, thus it requires amplification with a low noise amplifier prior to its entry into the input port. To reduce the coherent backscattering, the minimum input angle reflection at vertical polarization was obtained using different quasi-optical methods. After considering the results obtained using these methods, we measured the backscattering S_{11} by inserting the SRA plates at Brewster angle on a quasi-optical system.

A. Measurement of Brewster Angle for the SRA

1) Brewster Angle Measurement Using a Quasi-Optical System: To validate the performance of a quasi-blackbody plate using Eccosorb MF-110, the power reflection coefficient was measured at different incident angles. The S_{21} measurement setup comprised a quasi-optical system to measure the reflection loss at different angles of incidence, as shown in Fig. 2.

Fig. 2 shows the transmitting and receiving antennas of the diagonal horn connected to a vector network analyzer (VNA; Keysight Technology, PNA-X N5247A). In principle, the system can be extended to other frequency ranges between 325 and 500 GHz. In this case, the operating signal frequency of the VNA instrument set by the antenna was 480 GHz. The 480 GHz beam from the extender transmitter was transformed by the first parabolic mirror into a parallel configuration (collimated) before being rotated by 90°. A pair of wire grids and polarization rotator was used as a polarizer. The wire grid for clean-up polarizer is an optical component as a part of the polarizer. It was placed between the polarization rotator and the parabolic mirror. The polarization in the upward direction could be transmitted through the grid, while the polarization in the

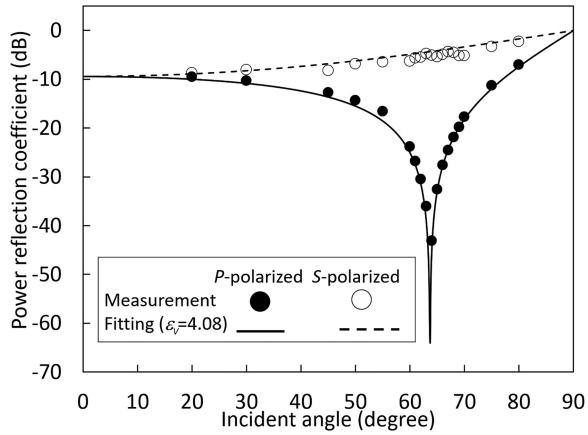

Fig. 3. Measured power reflection coefficients for incident beams with *p*-polarization (filled symbols) and *s*-polarization (open symbols). The Brewster angle is 63.7°, and ε_V is 4.08.

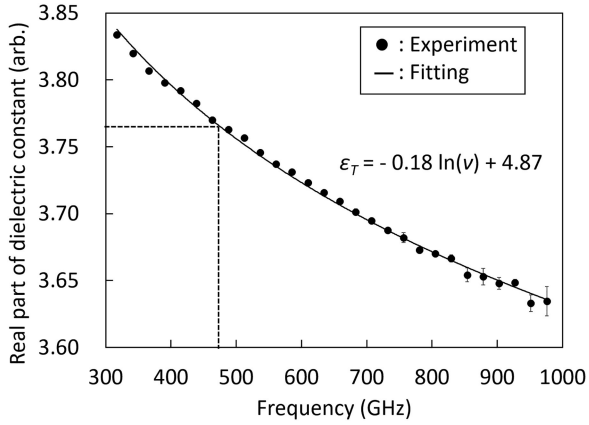

Fig. 4. Measured and fitted real parts of ε of the specular-reflection absorber plate, as determined using a THz-TDS.

sideways direction is reflected and excluded. The polarization rotator was a device that controls the direction of polarization by combining three reflectors, which were rotated in unison with respect to the axis of the beam common to the input and output as the rotation axis. The output polarization was at an angle of 2° with respect to the input polarization. At 0° of the polarization rotation angle, the directions of the input and output polarizations were equal. Moreover, the output polarization at 45° was orthogonal to the input polarization. The incident polarization is linear, generated by the *p*- or *s*-polarized incident beams after passing through the polarization rotator. The 3.0-mm-thick SRA plate is located on the sample stage. In Fig. 2, we show the beam passing through the first set of mirrors: a fixed ellipsoidal mirror for the polarized beam and the combination of a flat and ellipsoidal mirror for a beam polarized at an arbitrary angle. The polarized beam was irradiated onto the sample stage at an arbitrary incident angle, and then transmitted to the signal receiver as an electrical signal.

Fig. 3 shows the angular distributions of the power reflection coefficients for a THz incident beam of 480 GHz. By moving the arm to give an angular resolution, 18 data points for measuring angular incident distributions from 20° to 85° were obtained for both the *p* and *s* polarization planes. The incident angle has a measurement error of 0.1–0.3°. Generally, the imaginary part (ε_i) of the complex dielectric constant is associated with dielectric loss, which is minimal. The material loss limits the local minimum at the *p*–polarizer, as shown in Fig. 3. However, the Brewster angle, which is dependent on the incident angle, cannot be defined as the reflection of p-polarization (R_p) with ε_i [27]. Therefore, the Brewster angle should be defined as the incident angle of $R_p = 0$ at $\varepsilon_i = 0$. The real part of the complex dielectric constant is obtained from the VNA experiment (ε_V) and was found to be 4.08 by fitting the measurement data to (6) and (7), and the coefficients of determination R^2 for *p*- and *s*-polarization were 0.99 and 0.61, respectively. The resulting Brewster angle, given by $\tan(90^\circ - \theta) = \frac{1}{\sqrt{\varepsilon}}$, is calculated to be $\theta \approx 63.7^\circ$. In our observations, the local minimum for p-polarization was observed at 64.0° to be –43 dB. Based on the fit, the reflectivity was *-inf* dB at the Brewster angle (63.7°). It should be noted that the SRA exhibited an infinite thickness, and the loss tangent was neglected in the fitting model. However, the null at the Brewster angle should be less deep for lossy materials, therefore the local minimum for p-polarization can be considered to be ≤ -43 dB at $63.7^\circ \pm 0.3^\circ$.

2) THz Time-Domain Spectrometer Measurements: The Brewster angle for 480 GHz radiation was directly obtained with a quasi-optical reflectometer as a specular-reflection absorber. The dielectric property was measured using a THz time-domain spectrometer (THz-TDS) to investigate the mechanical errors in the setup. The measured value can be indirectly derived from the Brewster angle. The THz-TDS was a commercially available femto-second fiber laser (Tochigi Nikon Co., Rayfact SpecTera RS-01020). The THz-TDS method obtained the refractive index and absorption coefficient of the sample from the electric field of the transmission or reflection waves by introducing a THz signal into the sample [28]. This technique is common in microwave band measurements [29], [30]. The spectrum was measured using the reflection measurement method based on the significant absorption of electromagnetic waves by the sample.

The real part of ε versus frequency ν [GHz] between 300 and 1000 GHz is shown in Fig. 4. The real parts of the complex dielectric constant from the THz-TDS experiment (ε_T) decrease with increasing ν. Twenty-eight data points were fit using a simple exponential function. The permittivity given by $\varepsilon_T = -0.18 \ln(\nu) + 4.87$ and with at $\nu = 480$ GHz, was calculated as $\varepsilon_T = 3.77$. The permittivity of the imaginary part, given by $\varepsilon_{Ti} = 0.07 \ln(\nu) - 0.14$ was calculated to be $\varepsilon_{Ti} = 0.27$ at $\nu = 480$ GHz. Our measurement results represent only the real part of ε for refraction because the imaginary components are negligible. In other words, it does not have a significant effect on the Brewster angle given its magnitude. Previous studies reported that the characteristics of Eccosorb CR110 were equivalent to those of MF-110, and very little change in the dielectric constant occurs at higher frequencies up to 140 GHz and between 624 and 650 GHz [23], [31]. Our experimental result is in reasonable agreement with the dielectric constants at higher frequencies. The Brewster angle (θ) given by (5) was calculated from the fitting parameter

$\varepsilon_T = 3.77$. The measurement of θ calculated for ε was 62.7°, differing from the value calculated for ε_V reported in the previous section (63.7°). This difference may be because the transmission depends on the plate thickness, with only 0.89% transmission for a 3.0-mm-thick SRA plate. However, the measurement result confirms the angle accuracy up to the first decimal place at 480 GHz from the error of the 1σ values of the Brewster angle. As previously mentioned, a comparison between the results of this study and those of previous studies showed that the Brewster angle is frequency dependent.

B. Reflection Loss Measurement of the Double Brewster Angle (CHL) Configuration

1) Restrictions on the First SRA Angle Setting: The indentation accuracy (resolution) of the stepper motor was dependent on the position of the incident angle. As discussed in Section III, the CHL unit employs a mechanism in which the SRA and reflector mirror are in a back-to-back configuration.

During the calibration, the SRA was set at a suitable angle to minimize the reflection of the incident radiation. The default position of the SRA was taken to be 90°. Then, the motor can move the SRA away from 90° in discrete increments of 1.8°. The calibration Brewster angle of the SRA was set between 45° and 90°, as derived from the following equation:

$$\theta_{SRA} = 1.8\,(75 - m) \tag{8}$$

where θ_{SRA} [degree] is the calibration angle of the SRA plate using a two-phase stepper motor and the number of steps m is a natural number $25 < \mathrm{m} < 75$. It was reported in the previous section that the Brewster angle at 480 GHz is approximately 62.7°. According to (8), closest of θ_{SRA}, corresponds to $\mathrm{m} = 40$. We therefore used to use the motor to position the SRA at this angle, which approximated the Brewster angle.

2) Reflection Measurement Using the Quasi-Optical System: To obtain the performance of the MF-110 plate sample, it was also necessary to measure the *RL* at 63.0°. In this case, the *RL* for the SRA plate sample was measured from 450 to 500 GHz at increments of 0.01 GHz.

The terahertz CW transmitter and receiver (Extender Module for VNA) were connected to the VNA, as shown in Fig. 5. The basic structure is the same as that in Fig. 2. After designing the beam transmission system, the setup configuration is enclosed by a chamber lined with absorber material to prevent any interior reflection from surrounding objects within the chamber. The input intensity gain from the transmitter was approximately 40 dB in the form of a Gaussian beam with a beam waist radius of 13 mm. The cross-sectional areas of the beam are sufficiently smaller than those of the RAM and SRA. The irradiation sensitivity to the outside beam has negligible effects as losses are in the range of tens of dB. The antenna was used to illuminate the target at the Brewster angle by using a combination of an elliptical reflection mirror and a moving elliptical mirror.

Sample A was SRA-Al-SRA, while sample B was Al-RAM-RAM (see Fig. 5). In addition to the calibration targets, we measured the reference *RL* from a flat aluminum plate as a total reflector. Two aluminum mirrors on A and B were used

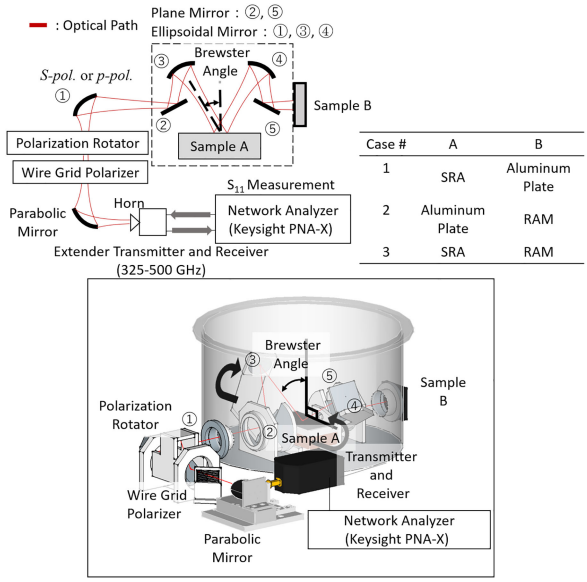

Fig. 5. Setup used to measure the optimal Brewster angle (minimizing S_{11}) of the SRA plate, including the setup of the quasi-optical reflectometer utilized to measure the reflection at the Brewster angle.

as reference baselines for 0 dB [19]. Using a set consisting of an SRA plate and RAM, we determined the input return loss (*IRL*) to demonstrate the feasibility of the compact design.

Fig. 6(a) shows the coherent backscattering S_{11} measurements for two single absorbers, SRA and RAM, and a combination of these absorbers. Between 450 and 500 GHz, the insertion loss of SRA with a thickness of 3 mm is −30 dB, whereas backscattering loss of RAM is approximately −50 dB. Case 1 in Fig. 6(a) was modified to represent the reflection loss of a single SRA reflection. Although the measured data shown in Fig. 3 was –36 dB at 63.0°, the arm of the setup angle represents an error of 0.1–0.3°. Therefore, an angle difference in the order of one-tenth of 63.0°, as shown in Fig. 3, resulted in a difference of several tens of decibels. In particular, the results of case 1 were –43 dB at 64.0° and –36 dB at 63.0°, as shown in Figs. 6(a) and 3, respectively. Cases 2 and 3 in Fig. 6(a) were displayed as time domain diagrams for Fig. 6(b) and (c), respectively. The horizontal axis represents time, where 0 ns corresponds to the position of the horn. The positions of sample A at 1.25 m and sample B at 1.81 m are circled. As shown in Fig 6(b), when sample A was an aluminum plate, the reflection decreased below –97 dB in this area. Further, as shown in Fig. 6(c), the reflection from sample B (RAM) was –110 dB, however, the backscatter from sample A (SRA) was –78.2 dB. Thus, most of the reflections were due to the SRA, and a portion of the backscatter may be due to the reflections from the various instruments around sample A. Although some peaks present in the TDF spectrum are not related to the sample A & B positions in Fig. 6(b) and (c), we consider that these peaks of less than –60 dB are part of the spurs. Therefore, most of the reflections in Fig. 6(c) are from the SRA, and the reflections in the direction of the specular reflection by SRA is –30 dB, while the reflection in the direction of the back scatter is –78 dB. The *RL* of the CHL does not become less than about –78 dB in the direction of the initial SRA backscatter.

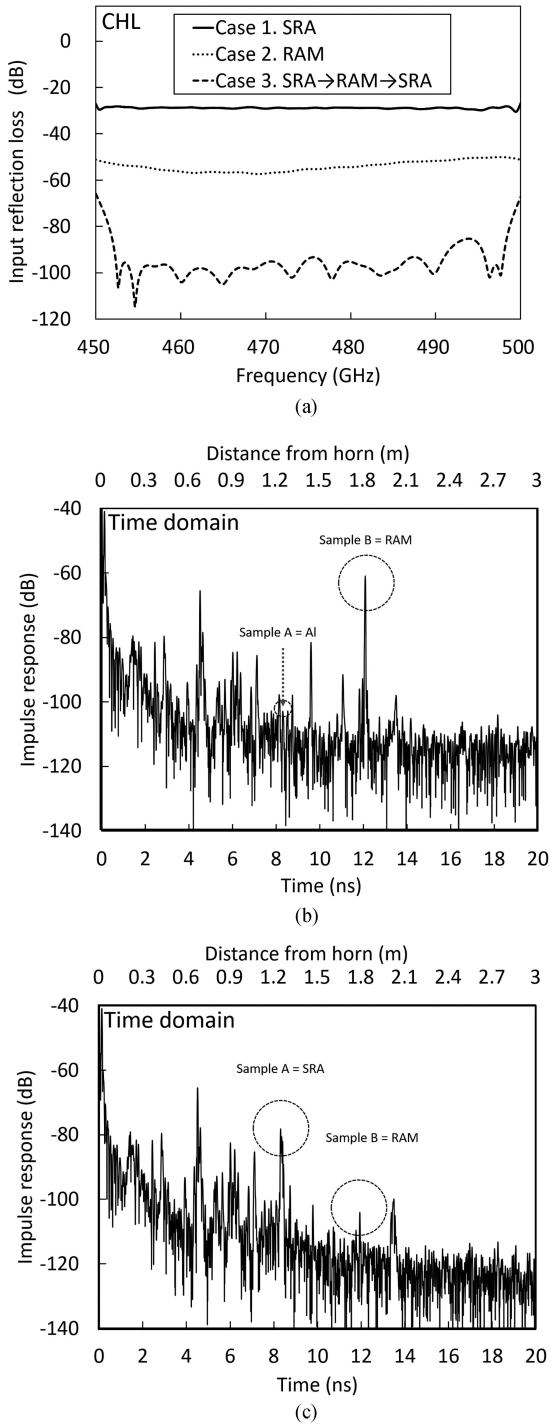

Fig. 6. (a) Reflection loss (*RL*) measurements of the CHL unit at 480 GHz and other absorbing materials at different frequencies between 450 and 500 GHz, respectively. Time domain reflectometry (TDR) measurements of reflections from various scatters in the beam propagation path for (b) case 2 and (c) case 3. The time axis represents the two-way travel time between the horn and the individual scatters.

However, the CHL design is expected to produce an intensity less than −60 dB at 480 GHz. Thus, the calibration system proposed in this study can be used in the CHL unit.

Fig. 7 shows the outside of the prototype and reflection absorbers for the THzSens receiver. To minimize the coherent

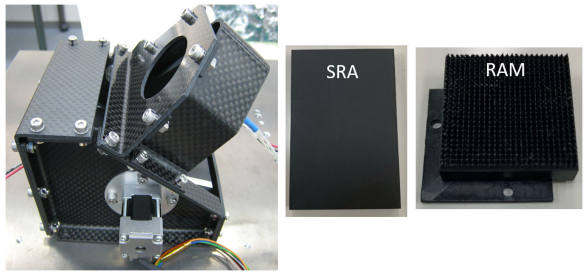

Fig. 7. Picture of the prototype CHL and reflection absorber for the THzSens receiver.

TABLE I
SUMMARY OF CHL UNIT SPECIFICATIONS FOR EACH MISSION

	THzSens requirements	THzSens CHL	SMILES CHL
Volume (cm^3)	$< 1.25 \times 10^5$	≤ 512	4.816×10^3 (total payload < 1.60×10^6) [a, b]
Mass (kg)	< 30	≤ 0.4	1.5 (total payload < 500) [a, b]
Frequency (GHz)	475.64 - 487.64	480	640 (system 624.32-650.32) [a, b]
CHL reflection loss (dB)	≤ -60	<−78	≤ -60 [c]
CHL housing	-	CFRP	Aluminum alloy [d]
CHL number of SRA plates	-	2	3 [a]

References: a. [23], b. [4], c. [32], d. [33]

backscattering radiation reflectivity for both polarization components, the angle of incidence with respect to the first SRA was set to the Brewster angle, 63.0°. From the measurement results, we observe that the attenuation of the proposed CHL design is −50 dB for the RAM, –30 dB for the first SRA, and it was expected to be more than –30 dB for the second SRA. Including the SRA back scattering, the CHL shows −78.2 dB of a total insertion loss. By arranging the SRA perpendicular to each polarization component, the coherent backscattering for each polarization component can be minimized.

Table I summarizes the major design specifications of the CHL unit for the THzSens. To compare the SMILES mission with the THzSens, previous CHL unit specifications are also included. To facilitate the planned manufacturing of the CHL unit, the table summarizes six parameters used to evaluate the CHL unit design. For the THzSens mission, the CHL unit design is based on top-down specifications for the volume and mass. The reflection loss results from this study will be useful for achieving the required physical properties of the microsatellite.

V. CONCLUSION AND FUTURE WORK

This article proposes a compact blackbody calibration unit design for a 480 GHz THzSens receiver to be mounted on a microsatellite to observe the emission lines of H_2O and O_2 in the atmosphere. The very low backscattering calibration unit, called the CHL unit, is designed to be lightweight and compact,

using only two SRA plates and a RAM as the absorber termination. The volume is approximately 1/10 of SMILES CHL. A lightweight CFRP material is also applied to the fixed materials for the absorber. The measured coherent backscattering S_{11} is less than –78 dB including SRA back scattering. The absorber combinations for the CHL design fulfill the specific THzSens requirements of $<$ –60 dB. We presented the results obtained from measurements with a quasi-optical compact design using a combination of absorbers. In future work, the performance of a manufactured prototype calibrator will be verified. Such experiments are in the process, using a prototype calibrator consisting of a RAM, two SRAs, and a stepper motor in a housing box of CFRP (see Fig. 7). Moreover, the reflectivity of the prototype calibrator will be examined using the transmitter/receiver setup employed in this study.

REFERENCE

[1] T. Ishikawa *et al.*, "On-orbit performance of High Temperature Noise Source (HTS) for advanced microwave scanning radiometer 2 (AMSR2) onboard the GCOM-W satellite," in *Proc. IEEE Geosci. Remote Sens. Symp.*, Jul. 2017, pp. 522–525.

[2] N. Liu and J. Ya-Qiu, "Average brightness temperature of lunar surface for calibration of multichannel millimeter-wave radiometer from 89 to 183 GHz and data validation," *IEEE Trans. Geosci. Remote Sens.*, vol. 59, no. 2, pp. 1345–1354, Jun. 2020.

[3] J. W. Waters *et al.*, "The earth observing system microwave limb sounder (EOS MLS) on the Aura satellite," *IEEE Trans. Geosci. Remote Sens.*, vol. 44, no. 5, pp. 1075–1092, May 2006.

[4] SMILES Mission Team, "SMILES Mission Plan," Nov. 2002, ver2.11. [Online]. Available: http://smiles.tksc.jaxa.jp/document/SMILES MP ver2.11.pdf

[5] N. P. Carleton and W. A. Traub, "Detection of molecular oxygen on Mars," *Science*, vol. 177, no. 4053, pp. 988–992, Sep. 1972.

[6] T. Owen, K. Biemann, D. R. Rushneck, J. E. Biller, D. W. Howarth, and A. L. Lafleur, "The composition of the atmosphere at the surface of Mars," *J. Geophys. Res.*, vol. 82, no. 28, pp. 4635–4639, Sep. 1977.

[7] P. Hartogh *et al.*, "Herschel/HIFI observations of Mars: First detection of O_2 at submillimetre wavelengths and upper limits on HCl and H_2O_2," *Astrophysics*, vol. 521, Jul. 2010, Art. no. L49.

[8] P. R. Mahaffy *et al.*, "Abundance and isotopic composition of gases in the martian atmosphere from the curiosity rover," *Science*, vol. 341, no. 6143, pp. 263–266, Jul. 2013.

[9] D. W. Davies, "The vertical distribution of Mars water vapor," *J. Geophys. Res., Solid Earth*, vol. 84, no. B6, pp. 2875–2879, Jun. 1979.

[10] C. R. Webster *et al.*, "Background levels of methane in Mars' atmosphere show strong seasonal variations," *Science*, vol. 360, no. 6393, pp. 1093–1096, Jun. 2018.

[11] R. D. Wordsworth, "The climate of early Mars," *Ann. Rev. Earth Planet. Sci.*, vol. 44, pp. 381–408, Jun. 2016.

[12] A. V. Rodin, O. I. Korablev, and V. I. Moroz, "Vertical distribution of water in the near-equatorial troposphere of Mars: Water vapor and clouds," *Icarus*, vol. 125, pp. 212–229, Jan. 1997.

[13] L. Maltagliati, F. Montmessin, A. Fedorova, O. Korablev, F. Forget, and J. L. Bertaux, "Evidence of water vapor in excess of saturation in the atmosphere of Mars," *Science*, vol. 333, no. 6051, pp. 1868–1871, Sep. 2011.

[14] R. T. Clancy *et al.*, "Vertical profiles of Mars 1.27 μm O_2 dayglow from MRO CRISM limb spectra: Seasonal/global behaviors, comparisons to LMDGCM simulations, and a global definition for Mars water vapor profiles," *Icarus*, vol. 293, pp. 132–156, Sep. 2017.

[15] J. H. Booske *et al.*, "Vacuum electronic high power terahertz sources," *IEEE Trans. Terahertz Sci. Technol.*, vol. 1, no. 1, pp. 54–75, Aug. 2011.

[16] Y. Kasai *et al.*, "Overview of the Martian atmospheric submillimetre sounder FIRE," *Planet Space. Sci.*, vol. 63, pp. 62–82, Apr. 2012.

[17] R. Larsson *et al.*, "Mars submillimeter sensor on microsatellite: Sensor feasibility study," *Geosci. Instrum. Methods Data Syst.*, vol. 7, no. 4, pp. 331–341, Dec. 2018.

[18] R. Takahashi, R. Sakagami, A. Wachi, Y. Kasai, and S. Nakasuka, "The conceptual design of a novel, small and simple Mars lander," in *Proc. IEEE Aerosp. Conf.*, Mar. 2018, pp. 1–10.

[19] A. Murk, N. Kampfer, R. Wylde, J. Inatani, T. Manabe, and M. Seta, "Characterization of various quasi-optical components for the submillimeter limbsounder SMILES," in *Proc. 12th Int. Symp. Space Terahertz Technol.*, Feb. 2001, pp. 426–435.

[20] Y. Iida, K. Kikuchi, T. Nishibori, A. Okabayashi, and T. Manabe, "Space-borne submillimeter wave calibration load with specular absorbers," *J. Remote Sens. Jpn.*, vol. 33, no. 2 pp. 109–116, Sep. 2013.

[21] A. Murk *et al.*, "Development of microwave calibration targets for upcoming ESA missions," in *Proc. IEEE Geosci. Remote Sens. Symp.,* Jul. 2012. pp. 2949–2952.

[22] K. Jacob, A. Schröder, and A. Murk, "Design, manufacturing, and characterization of conical blackbody targets with optimized profile," *IEEE Trans Terahertz Sci Technol* ., vol. 8, no. 1, pp. 76–84, Jan. 2018.

[23] R. Wylde, G. Bell, A. McNamara, and A. Murk, "The need for and development of MM-wave radiometer calibration targets with very low coherent backscatter," in *Proc. IEEE Conf. Precis. Electromagn. Meas* ., Jul. 2012, pp. 260–261.

[24] E. M. Berkhuijsen, "A consistent scheme of definitions of polarisation brightness temperature and brightness temperature," *Astron. Astrophys.*, vol. 40, pp. 311–316, Mar. 1975.

[25] P. Baron *et al.*, "Simulation study for the Stratospheric Inferred Winds (SIW) sub-millimeter limb sounder," *Atmos. Meas. Tech.*, vol. 11, pp. 4545–4566, Mar. 2018.

[26] S. Cloude, *Polarisation: Applications in Remote Sensing*. Oxford, MS, USA: Oxford Univ. Press, 2009.

[27] J. B. Götte and M. R. Dennis., "Generalized shifts and weak values for polarization components of reflected light beams," *New J. Phys.*, vol. 14, no. 7, 2012, Art. no. 073016.

[28] S. Saito, A. Syouji, K. Fukunaga, M. Mizuno, and I. Hosako, "Wide-band terahertz time domain spectroscopy for organic materials," in *Proc. IEEE Int. Conf. Solid Dielect.*, Jul. 2007, pp. 685–687.

[29] H. Yasuda and I. Hosako, "Measurement of terahertz refractive index of metal with terahertz time-domain spectroscopy," *Jpn. J. Appl. Phys.*, vol. 47, no. 3, pp. 1632–1634, 2008.

[30] K. B. Ng and C. H. Chan, "On the dielectric properties of substrates with different surface conditions for submillimeter-wave and terahertz applications," *THz Sci. Technol.*, vol. 9, no. 2, pp. 45–59, Jun. 2016.

[31] I. Zivkovic and A. Murk, "Characterization of magnetically loaded microwave absorbers," *Prog. Electromagn. Res.*, vol. 33, pp. 277–289, Jul. 2011.

[32] S. Ochiai *et al.*, "Performance of JEM/SMILES in orbit," in *Proc. 21st Int. Symp. Space THz Technol.,* Mar. 2010, pp. 179–184.

[33] S. Ochiai *et al.*, "Receiver performance of the Superconducting Submillimeter-Wave Limb-Emission Sounder (SMILES) on the international space station," in *Proc. IEEE Geosci Remote Sens. Symp* ., Jul. 2013, vol. 51, no. 7, pp. 3791–3802.

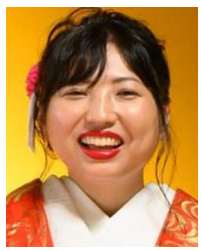

Maho Nakagawa received the Ph.D. degree in science from the Nagoya University, Nagoya, Aichi, Japan, in 2017.

From 2017 to 2018, she has been involved in experimental and development observation instrument with an organic aerosol reactivity of ambient air in atmospheric chemistry as program-specific Researcher and Assistant Professor. Since 2019, this experience led to her as Project Scientist with the National Institute of Communication and Technology, Tokyo, Japan, where she has been involved with a submillimeter-wave components and experimental study of atmospheric remote sensing instruments. Her current research interests include submillimeter-wave receiver development and high frequency measurement.

Dr. Nakagawa is a Member of the Japan Society of Atmospheric Chemistry and also a Member of the Japan Association of Aerosol Sciences and Technology.

Yuki Uchiyama received the B.E. and M.E. degrees in education from Tokyo Gakugei University, Tokyo, Japan, in 2018 and 2020, respectively.

He was a Trainee with the National Institute of Information and Communications Technology (NICT), Tokyo, Japan, in 2017. From 2018 to 2020, he has been a Cooperative Research Fellow with NICT. His scientific research interests include the submillimeter-wave devices and technology.

Takayoshi Yamada received the Ph.D. degree in science from the Tokyo Institute of Technology, Tokyo, Japan, in 2018, with developing submillimeter radiative transfer simulator including rotational non-LTE model and data analysis of remote sensing.

He is a Researcher with the National Institute of Information and Communications Technology (NICT), Tokyo, Japan. His scientific research interests include Terahertz radiative transfer modeling and remote sensing for Earth's and planetary atmosphere.

Toshiyuki Nishibori received the B.E. degree in instruments and control engineering from Hosei University, Tokyo, Japan, in 1987, and the M.E. and D.E. degrees in electrical and electronics engineering from Sophia University, Tokyo, Japan, in 1992 and 1995, respectively.

From 1987 to 1992, he was with Ishikawajima Harima Heavy Industries Co., Ltd. From 1995 to 1998, he was a Lecturer with the Tokyo Metropolitan College of Aeronautical Engineering, Tokyo, Japan.

He has been an Associate Researcher with the Institute of Space and Astronautical Science and engaged in the development of a time correction ground processing system for the Space Very Long Baseline Interferometry (Space VLBI). In 1998, he joined National Space Development Agency, where he is currently involved in the research and development of the Superconducting Submillimeter-Wave Limb-Emission Sounder to be aboard the Japanese Experiment Module of the International Space Station for observing stratospheric minor constituents related to ozone depletion. Since 2015, he has been the Senior Researcher of Sensor System Research Group, Research and Development Directorate, Japan Aerospace Exploration Agency. His current research interests include antenna design and measurements at frequency submillimeter-wave region, quasi-optics, radar remote sensing and ground penetrating radar.

Dr. Nishibori is a Member of the Japan Society for Aeronautical and Space Sciences and also a Member of the Astronomical Society of Japan.

Satoshi Ochiai received the B.E. and M.E. degrees in chemical engineering from Kyoto University, Kyoto, Japan, in 1986 and 1988, respectively.

In 1988, he joined the Radio Research Laboratory, which has been renamed into the Communications Research Laboratory a week after his employment and reorganized into the National Institute of Information and Communications Technology in 2004. Thereafter, he was engaged in research on millimeter and submillimeter-wave remote sensing. He was extensively involved in research with microwave radiometers in the institute, which include ground-based, balloon-borne, and spaceborne radiometers. His current research interests include the development of the millimeter-wave radiometer system and the calibration study of the microwave radiometer.

Maya Mizuno received the Ph.D. degree in engineering from Tohoku University, Sendai, Japan, in 2006.

In the same year, she joined the National Institute of Information and Communications Technology (NICT) as an Expert Researcher with the Applied Electromagnetic Research Institute and is currently a Senior Researcher.

Akihisa Uematsu received the B.E. degree in electric and electronics engineering from Kyoto University, in 2000, and the M.S. and Ph.D. degrees in informatics from Kyoto University, Kyoto, Japan, in 2002 and 2006, respectively.

From 2006 to 2009, he was an Expert Researcher with the National Institute of Information and Communications Technology (NICT). Since 2009, he joined the Japan Aerospace Exploration Agency (JAXA). He is currently an Associate Senior Researcher with the Sensor System Research Group of Research and Development Directorate, of JAXA, Tsukuba, Japan, where he is involved in research and development of terahertz and microwave instruments. His research interests are development and data analyses of spaceborne remote sensing active and passive microwave sensors and instruments, including synthetic aperture radars and radiometers.

Shigeru Sato received the M.S. degree in condensed matter physics from Tokyo Metropolitan University, Hachioji, Japan, in 1977.

He joined Konishiroku Photo Industry Co., Ltd. (Konica Minolta) as a Research Engineer from 1977 to 1985. He worked with Schlumberger Ltd. from 1985 to 2017 to develop measurement instruments for geophysical exploration used in oil wells. He is currently engaged in the development of a terahertz measurement unit for micro satellites with National Institute of Information and Communications Technology. His current interests include measurement algorithms using stochastic estimation theory.

Yukio Nakano received the Ph.D. degree in engineering from Kyoto University, Kyoto, Japan, in 2003, with kinetic and atmospheric chemistry.

He is an Associate Professor with the Department of Environmental Sciences, Tokyo Gakugei University, Tokyo, Japan. His scientific research interests include the chemical cycle of iodine in atmosphere and the development of teaching materials for the education of environmental issues.

Dr. Nakano is a Member of the Japan Society of Atmospheric Chemistry, the Chemical Society of Japan, Japan Society for Molecular Science, the Spectroscopical Society of Japan, the Japan Society for Science Education, and the Society of Japan Science Teaching.

Yasuko Kasai received the Ph.D. degree from the Department of Chemistry, Tokyo Institute of Technology, Tokyo, Japan, in 1995, with microwave molecular spectroscopy and radio astronomical observations.

She is an Executive Researcher with the National Institute of Information and Communications Technology (NICT), Tokyo, Japan. Her main work is at NICT, but she is also working at Tsukuba University. Her scientific research interests include satellite remote sensing for Earth's and planetary atmosphere.